

2
3
4
5
6

QUANTIFICATION OF MIXED-LAYER CLAYS IN MULTIPLE SATURATION STATES USING *NEWMOD2*: IMPLICATIONS FOR THE POTASSIUM UPLIFT HYPOTHESIS IN THE SE UNITED STATES

7 JASON C. AUSTIN^{1,2}, DANIEL D. RICHTER², AND PAUL A. SCHROEDER^{1*}

8 ¹Department of Geology, University of Georgia, Athens, GA 30602-2501, USA

9 ²Nicholas School of the Environment, Duke University, Durham, NC 27708, USA

10 **Abstract**—Quantification of mineral assemblages in near-surface Earth materials is a challenge because of the often abundant and highly variable crystalline and chemical nature of discrete clay minerals. Further adding to this challenge is the occurrence of mixed-layer clay minerals, which is complicated because of the numerous possible combinations of clay layer types, as defined by their relative proportions and the ordering schemes. The problem of ensuring accurate quantification is important to understanding landscape evolution because mineral abundances have a large influence on ecosystem function. X-ray diffraction analysis of the variable cation-saturated clay fraction in soil and regolith from the Calhoun Critical Zone observatory near Clinton, South Carolina, USA, was coupled with modeling using *NEWMOD2* to show that mixed-layer clays are often dominant components in the mineral assemblages. Deep samples in the profile (>6.5 m) contain mixed-layer kaolinite/smectite, kaolinite/illite-like, kaolinite-vermiculite, illite-like/biotite, and illite-like/vermiculite species (with 'illite-like' defined herein as Fe-oxidized 2:1 layer structure with a negative layer charge of ~0.75 per unit formula, i.e. weathered biotite). The 2:1 layers in the mixed layer structures are proposed to serve as exchange sites for K⁺, which is known to cycle seasonally between plant biomass and subsurface weathering horizons. Forested landscapes have a greater number of 2:1 layer types than cultivated landscapes. Of two nearby cultivated sites, the one higher in landscape position has fewer 2:1 layer types. Bulk potassium concentrations for the forested and two cultivated sites show highest abundances in the surface forested site and lowest abundance in the surface upland cultivated site. These observations suggest that landscape use and landscape position are factors controlling the mixed-layer mineral assemblages in Kanhapludults typical of the S.E. United States Piedmont. These mixed-layer clays are key components of the proposed mechanism for K⁺ uplift concepts, whereby subsurface cation storage may occur in the interlayer sites (with increased negative 2:1 layer charge) during wetter reduced conditions of the winter season and as biomass decay releases cation nutrients. Cation release from the mixed-layer clays (by decreased 2:1 layer charge) occurs under dryer oxidized conditions during the growing seasons as biota utilize cation nutrients. The types and abundances of mixed layers also reflect long-term geologic factors including dissolution/alteration of primary feldspar and biotite and the subsequent transformation and dissolution/precipitation reactions that operate within the soil horizons. Thus, the resulting mixed-layer clay mineral assemblages are often complex and heterogeneous at every depth within a profile and across landscapes. XRD assessment, using multiple cation saturation state and modeling, is essential for quantifying the clay mineral assemblage and pools for cation nutrients, such as potassium, in the critical zone.

32 **Keywords**—Biotite weathering · Critical zone observatory · Kanhapludult · Kaolinite · Mixed-layer clay · Potassium uplift

33
34

INTRODUCTION

35 Clay minerals are abundant and reactive components of the Earth's permeable surface that is influenced by meteoric waters (i.e. the Critical Zone), and can impact many aspects of ecosystems including soil fertility, ground water quality, and the fate and transport of contaminants (Schroeder 2018). More specifically, 2:1 and 1:1 hydrous layered phyllosilicates (clay minerals) have multiple structure sites in which to host (i.e. uptake/release) nutrients under different biogeochemical conditions, particularly those occurring along gradients developed by oscillations in moisture, redox potential, pH, and ion/complex activity (Hochella et al. 2019). The availability of K⁺ in a soil affects the composition of the suite of clay minerals present, with excess K⁺ resulting in increased abundance of 10 Å phases and paucity of K⁺ resulting in increased abundance of 17 Å phases (Officer et al. 2006; Barre et al. 2007b, 2008; Cornu et al. 2012). This adaptability of clay minerals in soil, to act as a source or sink for excess K⁺ under changing conditions, enhances the resilience of the soil to changing conditions.

56 One example of changing conditions is represented by the history of agriculture in the southeastern United States (SE US). In the late 18th century, portions of the Piedmont forest was cut and cultivated for agriculture (e.g. cotton), which, when combined with the region's temperate to subtropical climate, resulted in deep erosion and movement of top soils to the rivers (Trimble 2008). With the abandonment of SE US lands because of fertility loss, the landscape has since been vastly replanted in forest (often pine) with the perception by most that the ecosystem has recovered through the process of succession. This legacy of land use change has resulted in decreased root density in plots with a history of agriculture, with no roots present below 70 cm in currently cultivated plots (Billings et al. 2018). Suspected changes resulting from forest to row cropping also might include increased leaching rate of the soil, as the inputs from the surface would be removed (Balogh-Brunstad et al. 2008). The combination of these ef-

53
* E-mail address of corresponding author: schroe@uga.edu
DOI: 10.1007/s42860-019-00060-x

75 **Electronic supplementary material** The online version of this article (<https://doi.org/10.1007/s42860-019-00060-x>) contains supplementary material, which is available to authorized users. 76 77

fects, root removal and increased leaching, suggests that X-ray powder diffraction (XRD) patterns from the clay-fraction of cultivated-plot soils should show reduced abundance of 10 Å phases. Conversely, XRD patterns for the clay fraction of soils from plots which were forested continuously or replanted should show an increase in 10 Å phases. However, in these Piedmont soils, near surface weathering for at least 2.5 MY (Bacon et al. 2012) has left a high abundance of 1:1 layer clays which have no layer charge.

A common, and as yet poorly understood, aspect of clay mineral structure is the dynamics of mixed-layering in the clay minerals formed in weathered regolith and the role that it may play in the cycling of nutrients, particularly in landscapes that have been impacted by humans. The occurrence of mixed-layer minerals is especially important in kaolinite dominated soils, where the minor to trace abundances of 10, 14, and 17 Å phases play a pivotal role in the availability of nutrients for sustainable plant growth (Barre et al. 2008). The existence of mixed-layer minerals, and the complexity of their composition and formation pathways, especially in soil, has long been a topic of research. Generally, the most effectively agreed upon method for characterization is using multiple cation saturated specimens and computer modeling of XRD patterns from oriented mounts (Lanson et al. 2009; Dumon & Van Ranst 2016).

The purpose of the current study was to examine the structural state of mixed-layer clays in a comparative array of regoliths developed on different landscapes and land management scenarios in the SE US Piedmont as a proof of concept for using *NEWMOD2* to obtain meaningful and accurate quantification of mixed-layer clays. The approach was to use XRD to examine types of clay mineral structures and abundances that have been treated in the laboratory under varied cations saturation and hydration states. This method allows for the detection of mixed-layer clay structures by seeing differences in X-ray scattering properties. Accurate quantification of mixed-layer types can aid in the exploration of possible 2:1 layer exchange sites, which can serve as refugia for cationic forms of potassium and nitrogen (known essential nutrients for plant productivity). Integration of these datasets with others collected on the same samples will also allow for the exploration of the conditions under which mixed-layer clays form, and how they interact with the soil biota and pore water. The uplift of other ions (Mg, Ca, and P) and the nature of their vertical distributions are suggested to have important biogeochemical consequences (Jobbagy & Jackson 2004).

MATERIALS AND METHODS

Samples were collected from the Calhoun Critical Zone Observatory (CCZO) located in Union County, South Carolina, USA, as part of a multidisciplinary effort (Fig. S1. [Supplementary figures and tables are available from the Editor-in-Chief]). Related data sets for the CCZO are available and include listings for seasonal air and soil temperatures, climatic properties, LIDAR maps, groundwater and ground gas fluxes, photographs, soil properties, vegetative covers, and

streamflow fluxes (criticalzone.org/calhoun/data/datasets/). In summary, the region's annual precipitation averages 127 cm and the mean annual temperature is 15.7°C. The soils are composed of Cataula series (fine, kaolinitic, thermic oxyaquic Kanhapludults). Sites included in this study are pits located in experimental research watersheds that were excavated in 2016 using a backhoe to expose profiles down to ~3 m, which were intensively sampled. Deeper samples were extracted from the pits by hand auger to depths of ~8 m (Table 1). Cultivated plots in research watershed 1 (R1C) have been cultivated continuously with cover crops and occasionally amended with dolostone since 1930. Two pits excavated in R1C were considered in this study, with sites R1C2 and R1C3 located higher and lower, respectively, on the landscape. Research watershed 7 includes two pairs of forested plots (~15 m diameter) where all the trees have been identified, measured, and cored for age determinations. The forested plots were chosen with a hardwood plot that has been continuously forested, and a pine plot that was previously cultivated in each pair. Pits were dug in both sets of plots with the pit in pine plot #2 being the focus of this study (R7P2). Continuous sampling was conducted and bulk chemical and mineralogic analyses were performed for the profiles for all these sites, as well as four pits from two other watersheds; however, only a subset of shallow (<1 m) and deep (>6 m) samples were used from R1 and R7 as the focus for this current study (Table 1).

Samples were sieved to remove the >63 µm fraction and dispersed using a Branson Sonifier Cell Disruptor 350 (Branson Sonic Power Company, Danbury, Connecticut, USA) in a solution of 38 g Na-hexametaphosphate (Alfa Aesser, Ward Hill, Massachusetts, USA) and 8 g Na-carbonate (Baker Chemical Co., Phillipsburg, New Jersey, USA) per liter of deionized water. The clay fraction was separated to the <2 µm (equivalent spherical diameter) from the <63 µm fraction using centrifugation (Schroeder 2018). All samples were considered Na-saturated after this treatment. Approximately 1 g each of K-saturated and Mg-saturated sample were prepared by exchanging in 1.0 molar and 0.1 molar KCl (Fisher Chemical, Fairlawn, New Jersey, USA) and MgCl₂ (Acros, Morris Plains, New Jersey, USA) solutions, respectively. Exchanges were repeated by centrifugation and solution renewal to ensure full saturation. After rinsing of excess salt with deionized water, clay slurries were sedimented and air dried on 11 cm² glass petrographic slides to ensure infinite thickness (0.1 g/cm²). Each slide was scanned from 2–32°2θ (0.01° step and 0.1 s per step) using a Bruker D8 advance diffractometer (Bruker, Karlsruhe, Germany) with CoKα radiation (35 kV, 40 mA), goniometer radius of 21.7 cm, primary soller slits, 0.6 mm scatter slit, Fe-CoKβ filter, 2.5° receiving slit, and a Lynx-Eye position sensitive detector. Data were collected for each sample in the states of air-dried (AD), ethylene glycol (EG) (24 h at 20°C), and heated overnight at 110, 350, and 550°C. This multi-specimen method was similar to that effectively used by Lanson et al. (2009) on illite-smectites. Only the K- and Mg-saturated scans in the EG and 110°C state were considered for the comparison with calculated patterns, because the AD samples expressed multiple 0-

t1.1

Table 1 Sample locations and properties collected at the Calhoun CZO

Sample site	Depth (cm)	Cover type	Soil color	Latitude, Longitude	~Elevation (m)
R1C2	13–80	Cultivated	10 R 4/6	34.6114, –81.7279	184
R1C2	700–800	Cultivated	7.5 YR 4/6		177
R1C3	58–86	Cultivated	2.5YR 4/8	34.6092, –81.7279	177
R1C3	600–650	Cultivated	10YR 3/6		171
R7P2	57–82	Pine	2.5 YR 4/8	34.5412, –81.7541	162
R7P2	700–800	Pine	7.5TR 5/8		155

More detailed site descriptions and data for the above and related samples are available at criticalzone.org/calhoun/data/datasets/

190 water, 1-water, and 2-water hydrations states (see discussion
191 below).

192 Samples contained gibbsite (4.84 Å) and/or goethite (4.15
193 Å), which in each case allowed for correction of minor sample
194 displacement errors ($\leq \pm 0.05$ mm). Experimental data were
195 $K\alpha_2$ stripped using Bruker *Eva*[®] software (Version 4.2.0.14)
196 and exported in .xy format. A linear background was
197 subtracted from each data set using the minimum count per
198 second value and then imported as the experimental data into
199 *NEWMOD2*[®] software. *NEWMOD2* was used to model the
200 mixed-layer oriented XRD patterns (Reynolds 1980, 1985;
201 Yuan & Bish 2010). Tables S1a–f contain all *NEWMOD2*
202 model parameters used in the fitting for all XRD patterns.

203 A forward modeling approach was used, whereby param-
204 eters and abundances were adjusted to minimize the difference
205 between experimental and model patterns. Parameters adjusted
206 included: the d spacing of layer types, mean defect broadening
207 distance, high number (N) of coherent scattering domain (low
208 $N = 3$), ordering scheme (Reichweite), the percent of layer
209 types, and type abundance of exchangeable or fixed interlayer
210 cation in 2:1 structures, dioctahedral or trioctahedral layer type,
211 and abundance of octahedral iron in 2:1 structures. As
212 discussed by Austin et al. (2018), using a dioctahedral structure
213 is well suited to simulate the diffraction characteristics of
214 structural octahedral Fe in biotite that has undergone oxidation
215 from the ferrous to ferric state. The oxidation of Fe reduces
216 symmetry of the trioctahedral structure and makes the octahe-
217 dral site more dioctahedral-like in terms of XRD phenomena,
218 (i.e. shortening of the b lattice parameter), which has been
219 independently supported by far-infrared studies (Diaz et al.
220 2010). The layer charge must compensate for this loss by
221 expelling positive interlayer cations (i.e. potassium). If the unit
222 layer charge decreases from 1.0 to 0.75 then the structure
223 becomes ‘illite-like.’ Hence, for the purpose of this study and
224 modeling, the term ‘illite’ was used, following the convention
225 of Barre et al. (2007a). This is not meant to be the same as
226 authigenic illite formed during burial diagenesis or degraded
227 muscovite (Schroeder 1992).

228 The authors recognize that *NEWMOD2* accommodates
229 only two-layer types in model calculations and that, in nature,
230 three-layer type mixed-layer clays or combinations of the same
231 layer types in different hydration states may be present
232 (Dumon & Van Ranst 2016). Improvements to the current
233 approach could be made by modeling of 0-water, 1-water,

and 2-water layer types in 2:1 clay structures, particularly for
234 XRD patterns in the AD state. The results, however, indicated
235 that reasonably good simulations were possible in spite of this
236 limitation and the sample treatment differences were robust
237 enough to justify using the two-layer model. Using the fewest
238 variables in a model is beneficial for the eventual application of
239 clay mineral quantification in predictive capacities, such as
240 work by Hillier & Butler (2018) who predicted the extractable
241 potassium properties of soils from XRD data. Given the rea-
242 sonable goodness of fit results and the small visual difference
243 seen between both experimental and model data, the two-layer
244 model approach (i.e. *NEWMOD2*) was used.

245 Fits were assessed using Goodness of Fit (G), which was
246 calculated using the method described by Toby (2006) using
247 the equations:
248

$$R_{wp} = \sqrt{\frac{\sum_i w_i (y_{c,i} - y_{o,i})^2}{\sum_i w_i (y_{o,i})^2}} \quad (1)$$

$$R_{exp} = \sqrt{\frac{N}{\sum_i w_i (y_{o,i})^2}} \quad (2)$$

$$G = \frac{R_{wp}}{R_{exp}} \quad (3)$$

250 where y represents intensity values, w represents the
251 weight ($w = 1/\sigma^2[y_{o,i}]$, $\sigma^2[y_{o,i}] = y_{o,i}$), the subscript c
252 indicates calculated counts, and the subscript o indicates
253 measured counts of $i^2 2\theta$ (Austin et al. 2018).
254

255 The shorthand syntax suggested by Schroeder (2018) was
256 employed where the binary mixed-layer system is labeled
257 ABXXRY, where A = smaller d -spacing layer type, B = larger
258 d -spacing layer type, XX = percentage of layer A, and RY =
259 Reichweite ordering scheme when Y = 0, R is random ordering
260 and Y = 1, R is nearest neighboring layer only dependence. For
261 example, KS70R0 indicates kaolinite-smectite occurring with
262 70% kaolinite layer types, 30% smectite layer types, and
263 random ordering. If a layer type is repeated, then the structure
264 is considered a single structure (e.g. KK = pure kaolinite). In
265 some cases, modeling the same sample exposed to different
266
267
268
269
270

271 saturation and solvation states resulted in solutions where the
 272 layer types were the same, but the abundance of layer A vs B
 273 varied slightly. In these cases, the percentage of layer A (XX)
 274 was reported as a range of values. In other cases, the same
 275 sample exposed to different cation saturation and solvation
 276 states resulted in solutions where layer types and abundances
 277 changed. For *NEWMOD2* modeling purposes, the low and
 278 high number of coherent scattering domains and the mean
 279 defect free difference were varied in all cases (pure and
 280 mixed-layer phases) to minimize the difference between i_c
 281 and i_o .

282 To ensure accurate phase identification and quantification,
 283 XRD patterns of each sample under four different saturation
 284 and solvation states were modeled using *NEWMOD2*. During
 285 the modeling process, some theoretical considerations were
 286 required to ensure good fits that also made physical and
 287 chemical sense. Differences in the observed and modeled
 288 intensities at low angles ($2-7^\circ 2\theta$; $\sim 51-14$ Å) could be only
 289 partially explained by the theoretical parameters accommodated
 290 in the *NEWMOD2* model. The model mismatch for intensities
 291 at low angles sometimes resulted in modeled intensity
 292 being greater than the observed intensity. This was the case for
 293 all K-sat/EG solvated samples and all Mg-sat/EG solvated
 294 samples, except R12C3_600-650. In that case, a peak was
 295 observed at $\sim 4^\circ 2\theta$ (~ 25 Å) which was interpreted as illite-
 296 smectite. Three samples had observed intensities greater than
 297 modeled intensities (R1C2_13-80, Mg-sat/110°C & K-sat/
 298 110°C, and R1C3_600-650 K-sat/110°C).

299 This low angle intensity of the XRD pattern is influenced in
 300 part by the L_p factor. L_p is calculated by

$$L_p = \frac{1 + \cos^2 2\theta \psi}{2\theta} \quad (4)$$

302 where ψ is the powder ring distribution factor (Reynolds
 303 1986). Briefly, this factor can have either a single crystal
 304 or random powder form. If the random powder form is
 305 used, the preferred orientation of the sample has a large
 306 effect on the resulting low angle intensity. ψ is calculat-
 307 ed using the standard deviation of the assumed Gaussian
 308 distribution of tilt angles of the random powder (σ^*) and
 309 the size of the primary and secondary sollar slits
 310 (Reynolds 1986). Variations in σ^* cause the intensity
 311 at low angles to change, with higher σ^* values
 312 (representing more random orientation) resulting in
 313 higher intensity.

314 *NEWMOD2* parameters are able to model L_p are σ^* and the
 315 sollar slit sizes (primary and secondary). The sollar slit settings
 316 were kept constant throughout (6.6° primary and 2.5° receiv-
 317 ing) for all calculations. To evaluate the differences in the
 318 observed intensities across treatments, the average intensities
 319 for all treatments of all samples from each complete profile (n
 320 = 34 for each treatment) were compared (Fig. 1). In both cation
 321 saturation cases, the EG solvated samples had lower intensities
 322 in the low-angle region, thus indicating higher values for σ^*
 323 and implying that these samples were more randomly oriented

324 than the heated samples. As the samples were heated and the
 325 interlayer water and ethylene glycol were removed, the clay
 326 particles were assumed to behave in a manner that indicates
 327 more uniform orientation.

328 Reynolds (1986) determined that $\sigma^* = 12$ is a good esti-
 329 mation for oriented clay slides prepared as described above. In
 330 an attempt to resolve the differences between modeled and
 331 observed intensities, σ^* was adjusted during modeling. The
 332 calculation of G (Eq. 3) revealed negligible differences in
 333 quantitation as σ^* was varied. Therefore, a value of 12 for
 334 σ^* was used for consistency in the model fit for range of $2-7^\circ 2\theta$
 335 ($\sim 51-14$ Å) for samples in the Mg-sat/EG state
 336 (Table S1a-f).

337 In addition to differences observed in sample treatments,
 338 low-angle scattering was most pronounced in samples that in-
 339 cluded ordered mixed-layers and disordered smectitic mixed-
 340 layer minerals. This was attributed to mixed-layering, where the
 341 occurrence of quasi-super structures add intensity to the low-
 342 angle region. The lack of well defined higher order reflections
 343 that are expected in $>R1$ ordering make distinguishing between
 344 the effects of L_p and super structure low-angle scattering diffi-
 345 cult. Although beyond the scope of this study, this may be
 346 resolved through a systematic study of particle orientations using
 347 rocking curve experiments (Reynolds 1986).

348 The largest innovation to modeling mixed-layer clays pre-
 349 sented in this paper is the use of *NEWMOD2* for a systematic
 350 and quantitative comparison of mineral weight abundances
 351 (wt.%) across treatments. The method chosen for quantifica-
 352 tion required pre-assessment of various cation treatments and
 353 hydration states. This ensured that the suite of minerals pur-
 354 ported to exist had a sound physical basis across all sample
 355 treatment patterns. The mixed-layer minerals and quantity of
 356 layer types were compared across the sample treatments using
 357 the following criteria to identify and assess discrepancies:

- 358 (1) The total number of kaolinite layers could not change
 359 with solvation, saturation, or heating.
- 360 (2) Expanding layer types could be collapsed by heating and
 361 K saturation, causing an apparent increase in illite-like
 362 layers.
- 363 (3) Changes in the d spacing of expandable layers could
 364 result in an apparent increase in kaolinite mixed-layers
 365 as long as no increase occurred in the abundance of
 366 kaolinite layers.
- 367 (4) Treatments were not be expected to completely transform
 368 all 2:1 clay layers in a sample, e.g. some low charge
 369 smectite layers may not completely collapse to 10Å upon
 370 K saturation, resulting in an apparent increase in vermic-
 371 ulite layers.
- 372 (5) G values were minimized in compliance with the preced-
 373 ing rules.

374 In order to keep compliance with the criterion (1), methods
 375 for the abundance calculations were limited to those model
 376 solutions that best balanced each layer type for all treatment/
 377 hydration conditions. This resulted in a dynamic tabulation of
 378 layer-type abundances (Fig. 2) using the *NEWMOD2* solutions

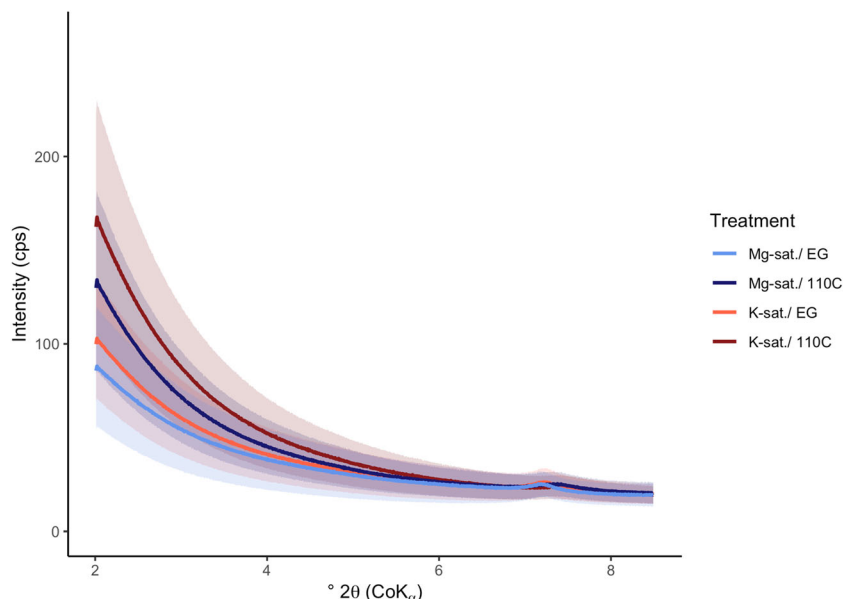


Fig. 1 Average XRD intensity (source = CoK α) of all samples grouped by treatment ($n = 34$ for each treatment). Color coded regions represent one standard deviation with blended shades showing overlaps. Heated samples exhibited greater low-angle scattering compared to their EG-saturated states. K-saturated samples exhibited greater low-angle scattering compared to the Mg-saturated states. This response can be attributed partly to sample-sensitive changes related to orientation and scattering behavior (Reynolds 1986). The increased low-angle scatter is consistent with a more powder-like Lorentz polarization (Lp) of the beam, whereas the decreased low-angle scatter, a more single crystal-like Lp of the beam. Differences in low-angle scattering can also be attributed to mixed-layering, where the occurrence of quasi-super structures add intensity to the low-angle region

379 for each state. The numbered arrows are intended to give a
 380 sense for the quantity of layers that were transformed during
 381 the heating treatment. In some cases, the transformation
 382 showed more kaolinite layers than expected. For example,
 383 the K-sat/110°C treatment of R7P2_700-800 had fewer than
 384 expected kaolinite layers as compared to the K-sat/EG treat-
 385 ment of R7P2_700-800. XRD patterns for R7P2_700-800 K-
 386 sat treatments showed, upon heating, no increase in intensity or
 387 asymmetry on the low-angle side of the peak at $14^\circ 2\theta$ (~ 7 Å),
 388 and a decrease in a broad area of higher intensity between 5
 389 and $10^\circ 2\theta$ (15–10 Å) centered around $7^\circ 2\theta$ (~ 14 Å) (Fig. S7).
 390 This is interpreted as a collapse of expandable, mixed-layer
 391 kaolinite-vermiculite (~ 7 Å/ ~ 14 Å) to kaolinite-illite (~ 7 Å/
 392 ~ 10 Å). This interpretation is consistent with the interpretation
 393 of the other treatments, though the best fit model (both visually
 394 and with the lowest G) results in more kaolinite layers than
 395 expected. A similar response was observed in the R1C2_700-
 396 800 K-sat patterns, with a slight decrease in intensity on the
 397 low-angle side of the broad peak at $10^\circ 2\theta$ (~ 10 Å) accompa-
 398 nied by an increase in both peak-width and intensity, on the
 399 low angle side of the $14^\circ 2\theta$ (~ 7 Å) peak (Fig. S3). Difficulties
 400 occurred in resolving *NEWMOD2* model solutions that consis-
 401 tently provided mass balance to layer transformations for
 402 the K-sat samples.

403 In contrast, the Mg-sat/EG treatment for all samples was
 404 considered more consistent than all the K-sat sample treat-
 405 ments for mass balancing the layer types upon heating (Fig.
 406 2). Differences in mixed-layer types manifested in K-sat states
 407 vs Mg-sat states were related to heterogeneous layer charges

408 within the 2:1 layers and resultant layer heterogeneous dimen-
 409 sions (Lagaly 1982; Gier et al. 1998). As noted by MacEwan &
 410 Wilson (1980), structural contractions of K-sat states in 2:1
 411 layers are variable in response to the amount of layer charge.
 412 The state of an octahedrally coordinated two-layer Mg-hydrate
 413 group $[\text{Mg}(\text{H}_2\text{O}_6)]^{2+}$ occupies a more uniform and consistent d
 414 spacing than K-sat states. Therefore, Mg-sat/EG were used for
 415 quantification.

RESULTS

416
 417 The diffraction patterns of the K- and Mg-saturated sam-
 418 ples in both the EG and 110°C states, respectively, showed
 419 small differences at high angles ($>20^\circ 2\theta$; <4.44 Å) (Fig. 3, S2–
 420 S7). All patterns for the same sample in the various states
 421 showed larger differences at low angles than at higher angles.
 422 The differences between the patterns for the same sample
 423 under different saturation and hydration states was most con-
 424 servatively explained by two factors. Firstly, sample sensitive
 425 modifications (i.e. Lorentz-polarization (Lp)) are associated
 426 with changes in orientation (Reynolds 1986) upon treatment.
 427 Secondly, specimen sensitive modifications are associated
 428 with the presence of mixed-layering caused by changes in:
 429 (1) types of layers, (2) proportions of layer types, (3) the
 430 dimensions of layer types, and (4) interlayer composition.

431 Forward models using *NEWMOD2* conformed well with
 432 experimental patterns (Figs. 4 and 5). These results conform
 433 with the constraint that the same sample treated under different
 434 cation saturation states (i.e. K^+ vs Mg^{2+}) and hydrations states

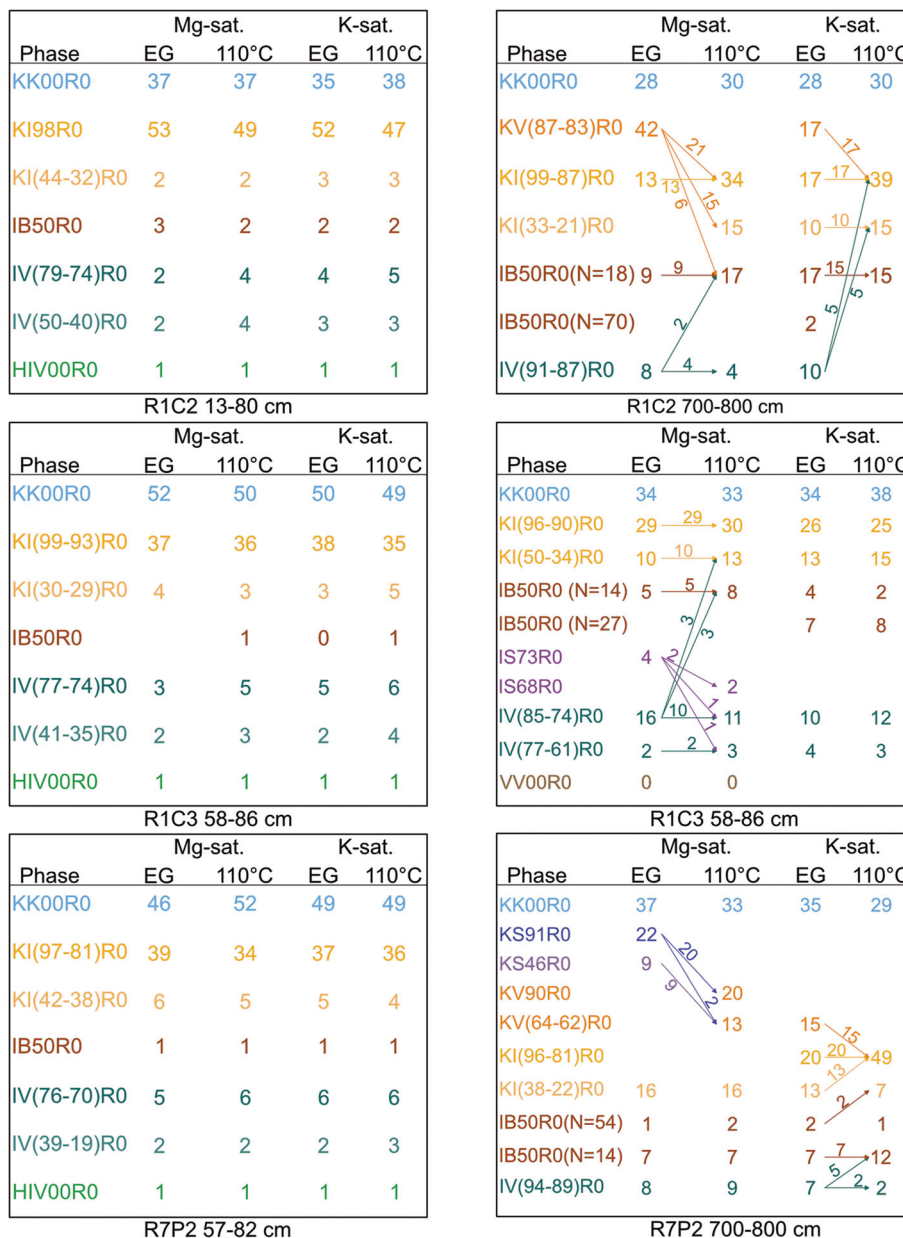


Fig. 2 Quantitative representation of changes in modeled layer type abundances based on changes in XRD patterns from different sample treatments (Table 2). Arrows depict the changes in layer types and abundances resulting from heat treatments. Values on the arrows quantitatively constrain the number of layer types transformed after heat treatment. Color codes show similar mixed-layer groups: kaolinite and kaolinite-smectite dominated (cool violet/blues), kaolinite-illite-like dominated (warm brown to yellows), and vermiculite dominated (greens). The shallow samples (left side) exhibited low abundances of expandable 2:1 layers in all profiles, resulting in relatively small but perceptible changes with treatments. Deep samples (right side) had more abundant/dynamic 2:1 illitic and expandable layers

435 (i.e. EG vs 110°C) are quantitatively balanced. The expected
 436 response for low charge 2:1 exchange sites (where unit layer
 437 charge = X , i.e. $0.3 < X < 0.45$) is that EG saturated d spacings
 438 for K^+ and Mg^{2+} states expand to $\sim 17.05 \text{ \AA}$ and $\sim 16.85 \text{ \AA}$,
 439 respectively. Upon heating to 110°C these layers collapse to
 440 $\sim 10 \text{ \AA}$. If the layer charges are higher (i.e. $0.45 < X < 0.75$),
 441 then K-saturated layers may expand to $\sim 17 \text{ \AA}$, which may be
 442 related to the relatively small enthalpy of hydration for K^+ ($-$

320 320 kJ mol^{-1}), whereas Mg-saturated layers expand to $\sim 14 \text{ \AA}$ 443
 443 due to larger enthalpy of hydration for Mg^{2+} ($-1921 \text{ kJ mol}^{-1}$). 444
 444 Enthalpy of hydration values were reported by Smith (1977); 445
 445 being defined as energy released by an ion in a large amount of 446
 446 water at 298°K and 1 atm. Layers that expand to $\sim 14 \text{ \AA}$ were 447
 447 modeled as vermiculite and layers that expand to $\sim 17 \text{ \AA}$ were 448
 448 modeled as dioctahedral smectite. Well ordered 10 \AA layers 449
 449 were modeled as discrete trioctahedral biotite ($X = 1.0$). 450
 450

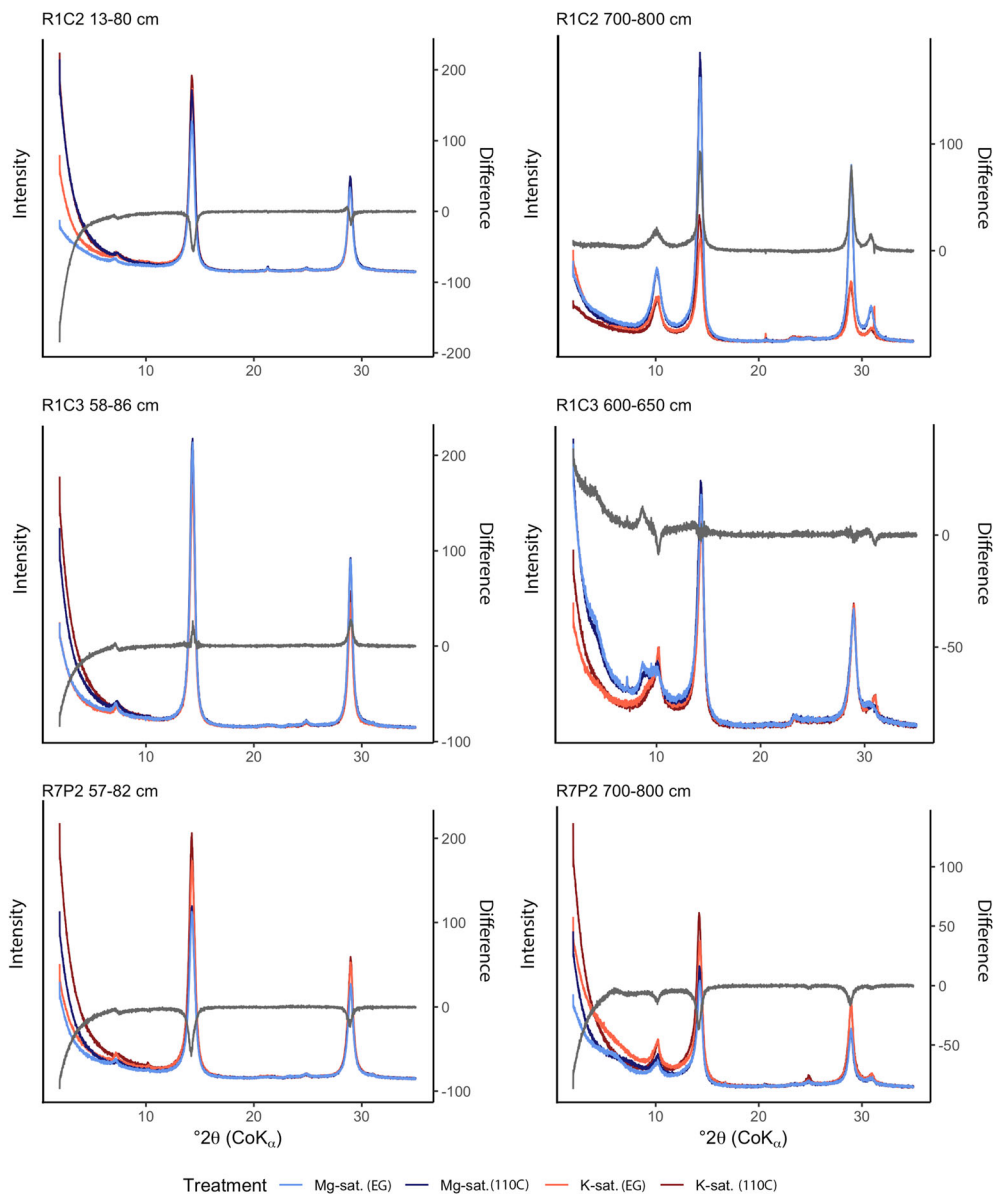


Fig. 3 XRD patterns for all treatments of all samples superimposed at the same relative intensities. The gray line represents the difference between the measured intensities (counts per second) of the Mg-sat./EG solvated sample and the average of differences for the other treatments (i.e. Mg-sat. (EG) - [(Mg-sat. (EG) - Mg-sat. (110°C) + (Mg-sat. (EG) - K-sat. (EG) + (Mg-sat. (EG) - K-sat. (110°C))]/3). Positive deflections signify that the influence of quasi-superstructures dominates scattering and the effect of orientation (Lp) is diminished. Negative deflections signify the absence of quasi-superstructures and the dominance of the orientation effect (Lp)

451 Based on numerous forward modeling efforts, 10 Å
 452 halloysite layer types were not used in calculated solutions
 453 as fits could not be improved with their inclusion, even
 454 though halloysite is common in Kanhapludults (Joussein
 455 et al. 2005). As discussed above, unaltered biotite was best
 456 modeled as a 10 Å trioctahedral mica with $X = 1.0$ using K
 457 in the interlayer and 1 mole ^{VI}Fe per formula unit. Weathered
 458 biotite was best modeled as dioctahedral mica with $X =$
 459 0.75 and 0.4 mole ^{VI}Fe per formula unit as illite-like
 460 layers. Hydroxy-interlayered vermiculite (HIV) was also
 461 found as a discrete phase in the shallow samples, which

exhibited a persistent ~ 14.2 Å reflection for EG saturated
 samples and slightly collapsed to a 13.8 Å d spacing after
 110°C treatment (Meunier 2007). HIV was best modeled in
 $NEWMOD2$ using trioctahedral chlorite.

Based on the possible layer types resulting from combina-
 tions of interlayer cation type, layer charge, and hydration
 states, the following layer types were quantified in the
 $NEWMOD2$ calculations: B = biotite (trioctahedral mica), I =
 illite-like (modeled with tri- and dioctahedral mica), K = kao-
 linite, S = smectite (modeled as trioctahedral in EG state), V =
 vermiculite (modeled as trioctahedral), HIV = hydroxy

462
 463
 464
 465
 466
 467
 468
 469
 470
 471
 472

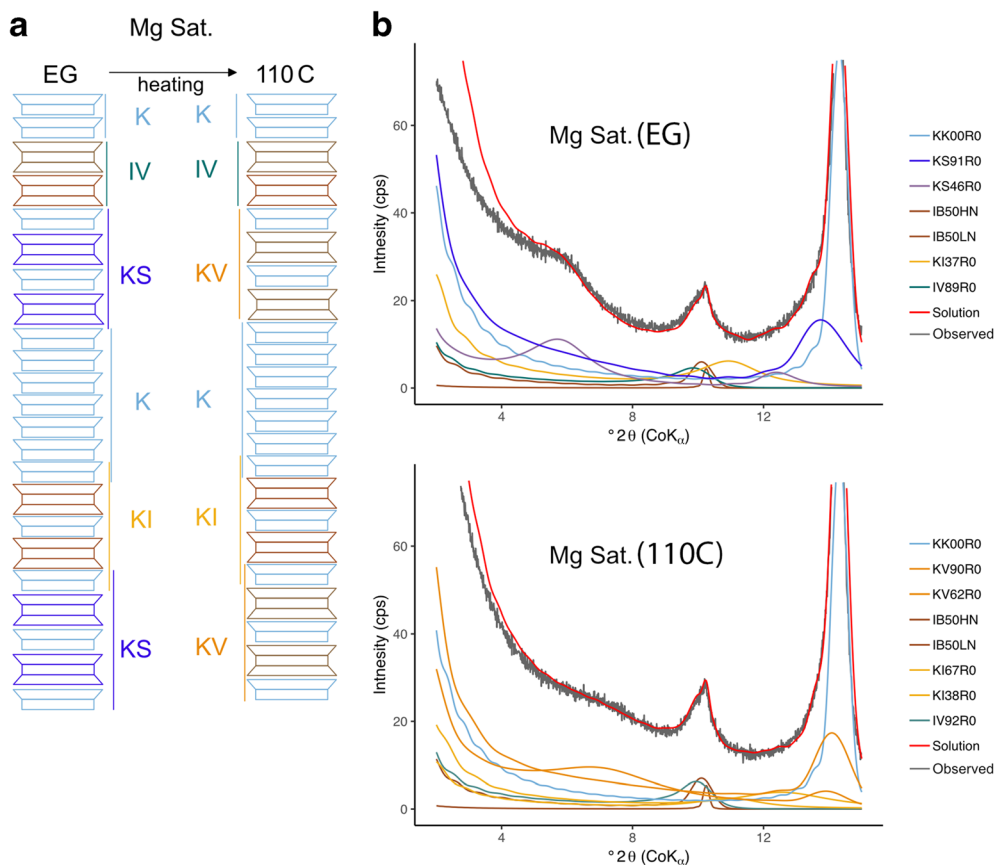


Fig. 4 Changes in low-angle regions of XRD patterns for R7P2_700-800 indicate the presence of mixed-layer minerals. (A) Schematic diagram of changes in the mixed-layer structure upon heating the Mg-sat. (EG) slide to 110°C. (B) NEWMOD solutions showing individual phases and the complete modeled pattern (red) compared to the observed pattern (gray) in EG state (upper) and 110°C state (lower)

473 interlayered vermiculite (modeled as tri- trioctahedral chlorite).
 474 *NEWMOD2* modeling results (summarized in Table 2) include
 475 specific values used for layer types, relative abundance, layer
 476 dimensions, low and high coherent scattering domain numbers,
 477 and mean coherent scattering domain size. Full details of
 478 all the *NEWMOD2* model parameter for every sample are
 479 presented in supplemental data (Tables S1a–f).

480 For the following discussions about each location, the
 481 samples will be referred to as shallow and deep within each
 482 profile, representing B-horizon and C-horizons (i.e. saprolite),
 483 respectively. Also, the results refer to the modeled abundances
 484 of mineral phases in the Mg-sat/EG states. Model solutions
 485 were calculated for the other states as discussed above in the
 486 methods section, but they were used primarily to ensure that
 487 the solutions derived for the Mg-sat/EG patterns were correctly
 488 mass balanced (i.e. the expected changes in *d* spacing with the
 489 various treatments were observed in the XRD patterns).

490 Research Watershed 1 Cultivated Sites

491 The most abundant mineral deep in the R1C2 profile was
 492 KV(87-83)R0 (42 wt.%), followed by kaolinite (8 wt.%),

493 KI(87-83)R0 (13 wt.%), IB50R0 (9 wt.%), and IV(91-87)R0
 494 (8 wt.%). In the shallow sample, the most abundant phase was
 495 KI198R0 (53 wt.%) with KK00R0 (37 wt.%) and minor
 496 amounts KI, IB, IV and HIV phases (<3 wt.%). Two popula-
 497 tions of IB were observed in R1C2 that were distinguished by
 498 differences in their mean CDS (67 vs 10; i.e. well ordered and
 499 poorly ordered, respectively). HIV was not detected in the deep
 500 R1C samples, which is consistent with the observations of
 501 Barnhisel & Bertsch (1989), who noted that HIV generally
 502 forms at shallow depths in the soil where aluminum activity is
 503 high. Also observed were a small percentage of KI(44-32)R0 (2
 504 wt.%) and an increase in KI98R0 from 13 wt.% to 53 wt.%,
 505 deep-to-shallow, respectively. Discrete kaolinite (KK00R0)
 506 was more abundant in the shallow sample than the deep sample.

507 Though the land use histories for sites R1C2 and R1C3 are the
 508 same, the mixed-layer clays and abundances are distinctly differ-
 509 ent in several ways. One notable example in the deep sample of
 510 R1C3 is a greater abundance of vermiculite layers. The
 511 *NEWMOD2* model solution included a discrete vermiculite phase
 512 because of a sharp 14 Å peak in the pattern, which indicated a
 513 large mean CDS. The reported Tr % indicated that the well
 514 ordered vermiculite was likely present in trace amounts, but the

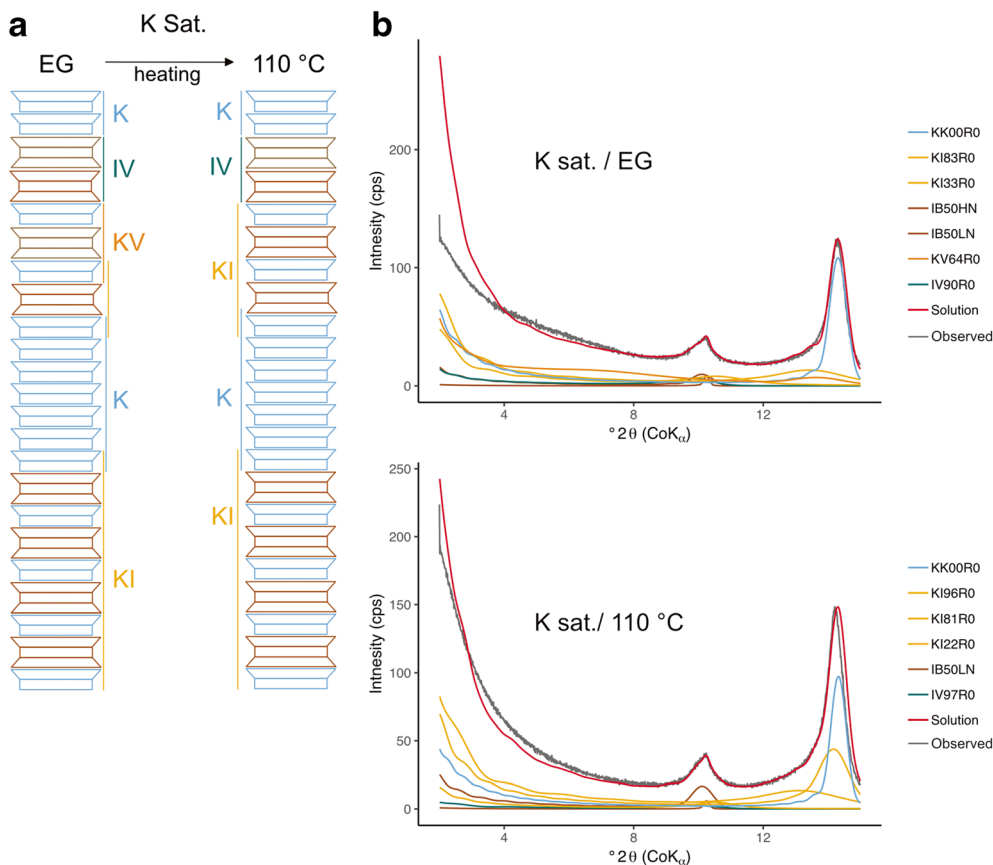


Fig. 5 Changes in low-angle regions of XRD patterns for R7P2_700-800 indicate the presence of mixed-layer minerals. (A) Schematic diagram of changes in the mixed-layer structure upon heating the K-sat. (EG) slide to 110°C. (B) NEWMOD solutions showing individual phases and the complete modeled pattern (red) compared to the observed pattern (gray) in EG state (upper) and 110°C state (lower)

515 abundance was too close to the detection limit using this method
 516 (Fig. S5). *NEWMOD2* quantification has up to $\pm 7\%$ relative error
 517 and ± 3 wt.% for layer-type abundance, which is based on repeated
 518 independent modeling of several samples by Austin et al. (2018).
 519 The deep samples also included two IS phases (IS73R0 and
 520 IS68R0) plus IV(77-61)R1 and IV(84-74)R0.

521 The shallow RIC3 downslope sample is distinct from the
 522 shallow RIC2 upslope sample where the relative abundance of
 523 kaolinite (52 wt.%) is greater than KI (41 wt.%) in RIC3, whereas
 524 the KI mixed-layer phase was more abundant than the kaolinite
 525 phase in RIC2. The abundances of the remaining phases in the
 526 shallow samples are comparable between RIC2 and RIC3.

527 *Research Watershed 7 Pine Site 2*

528 Deep in the forested profile (R7P2), two distinct forms of
 529 IB were found; one well ordered with a large mean CDS (47, 1
 530 wt.%) and one poorly ordered with small mean CDS (14, 7
 531 wt.%). Also observed were two KS phases that accounted for
 532 31 wt.%. Kaolinite layers were more abundant (37 wt.%) than
 533 IB layers (16 wt.%). The deep sample also contained IV(94-
 534 89)R0 (8 wt.%).

535 The abundance of kaolinite (46 wt.%) was greater than the
 536 KI phase (29 wt.%) in the shallow sample (as in the profile at
 537 RIC3). The abundances of IV mixed-layers (7 wt.%)

538 combined) and KI (5 wt.%) with a majority of illite-like layers
 539 were the greatest for all the profiles. Trace amounts of HIV and
 540 an illite-like phase were also present (1 wt.% each).

DISCUSSION

541
 542 Quantification of mixed-layer clay phases allows compari-
 543 son of the relative trends in clays as a function of land use and
 544 position in the depth profile, as proposed by Austin et al. (2018).
 545 Knowledge of the types of clay minerals present, especially with
 546 respect to their capacity to exchange cations with the biota and
 547 soil solution is fundamental for understanding the cycling of
 548 nutrients in the soil (see e.g. Lybrand et al. 2019). Areas such as
 549 the Calhoun CZO are perceived to bear only discreet clay-
 550 mineral assemblages (i.e. no mixed-layer clays). The present
 551 authors submit that, as a rule, although mixed-layer clays are
 552 not always abundant in soils, they are common in soils. Correct
 553 identification and accurate quantification of these mixed-layers
 554 requires careful and nuanced interpretations of oriented XRD
 555 patterns under variable saturation states. The combination of
 556 new paradigms for mineral-microbe relations (Lybrand et al.
 557 2019) and advances in XRD analytics now allow the quantita-
 558 tive importance of mixed-layer clays and their role in CZ eco-
 559 system function to be addressed. In particular, from the

t2.1 **Table 2** Modeled % Abundance of mixed-layer clays using *NEWMOD2*

		Modeled % abundance (wt.%)								
Sample	Phase*	Mg-EG	Mg-110C	K-EG	K-110C	D001A (Å)	D001B (Å)	Low N	High N	Mean CDS
R1C2_13-80	KK00R0	37	37	35	38	7.15	7.15	3	31	27
	KI98R0	53	49	52	47	7.15	10	3	23	17
	KI(44-32)R0	2	2	3	3	10	7.15	3	10	5
	IB50R0	3	2	2	2	9.98	10	3	8	12
	IV(79-74)R0	2	4	4	5	10	14.32	3	14	4
	IV(50-40)R0	2	4	3	3	10	14.32	3	14	4
	HIV	1		1		14.2	14.2	3	16	18
	HIV		1		1	13.8	13.8	3	14	13
Sample	Phase*	Mg-EG	Mg-110C	K-EG	K-110C	D001A (Å)	D001B (Å)	Low N	High N	Mean CDS
R1C2_700-800	KK00R0	28	30	28	30	7.15	7.15	3	35	27
	KI(99-87)R0	13	34	17	39	7.15	10	3	20	11
	KV(87-83)R1	42		17		7.15	14.32	3	14	16
	KI(33-21)R0		15	10	15	10	7.15	3	14	7
	IB50R0	9	17	17	15	9.98	10	3	18	10
	IB50R0			2		9.98	10	3	70	67
	IV(91-87)R0	8	4	10		10	14.32	3	14	7
Sample	Phase*	Mg-EG	Mg-110C	K-EG	K-110C	D001A (Å)	D001B (Å)	Low N	High N	Mean CDS
R1C3_58-86	KK00R0	52	50	50	49	7.15	7.15	3	36	30
	KI(99-93)R0	37	36	38	35	7.15	10	3	20	15
	KI(30-29)R0	4	3	3	5	10	7.15	3	14	6
	IB50R0		1	Tr	1	9.98	10	3	14	4
	IV(77-74)R0	3	5	5	6	10	14.32	3	14	3
	IV(41-35)R0	2	3	2	4	14.32	10	3	14	5
	HIV	1		1		14.2	14.2	3	17	17
	HIV		1		1	13.9	13.9	3	19	14
Sample	Phase*	Mg-EG	Mg-110C	K-EG	K-110C	D001A (Å)	D001B (Å)	Low N	High N	Mean CDS
R1C3_600-650	KK00R0	34	33	34	38	7.15	7.15	3	27	24
	KI(96-90)R0	29	30	26	25	7.15	10	3	14	10
	KI(50-34)R0	10	13	13	15	10	7.15	3	14	5
	IB50R0	5	8	4	2	9.98	10	3	14	14
	II00R0			7	8	9.98	10	3	27	27
	IS73R0	4				10	16.9	3	14	7
	IS68R0		2			10	12.4	3	14	8
	IV(85-74)R0	16	11	10	12	10	14.32	3	42	6
	IV(77-61)R1	2	3	4	3	10	14.32	3	23	11
VV00R0	Tr	Tr			14.32	14.32	3	61	106	
Sample	Phase*	Mg-EG	Mg-110C	K-EG	K-110C	D001A (Å)	D001B (Å)	Low N	High N	Mean CDS
R7P2_57-82	KK00R0	46	52	49	49	7.15	7.15	3	29	25
	KI(97-96)R0	39	34	37	36	7.15	10	3	19	13
	KI(42-38)R0	6	5	5	4	10	7.15	3	14	5
	IB50R0	1	1	1	1	9.98	10	3	33	32
	IV(76-70)R0	5	6	6	6	10	14.32	3	14	4
	IV(39-19)R0	2	2	2	3	14.32	10	2	6	4
	HIV	1		1		14.2	14.2	3	19	20
	HIV		1		Tr	13.9	13.9	3	16	16
Sample	Phase*	Mg-EG	Mg-110C	K-EG	K-110C	D001A (Å)	D001B (Å)	Low N	High N	Mean CDS
R7P2_700-800	KK00R0	37	33	35	29	7.15	7.15	3	26	24
	KI(96-81)R0			20	49	7.15	10	3	10	8
	KI(38-22)R0	16	16	13	7	10	10	3	14	6

t2.54 **Table 2** (continued)

Modeled % abundance (wt.%)									
KS91R0	22				7.15	16.9	3	11	9
KS46R0	9				7.15	16.9	3	8	11
KV90R0		20			7.15	14.32	3	11	12
KV(64-62)R0		13	15		7.15	14.32	3	8	10
IB50R0	1	2	2	1	9.98	10	3	54	47
IB50R0	7	7	7	12	9.98	10	3	14	14
IV(94-89)R0	8	9	7	2	10	14.32	3	14	7

*Layer types: K = kaolinite, I = illite-like (as defined in this study), V = vermiculite, S = smectite, HIV = hydroxy-interlayered-vermiculite, B = biotite, R = reichweite (0 = randomly ordered, 1 = ordered). N = number of coherent scattering domain range (Low to High), CDS is mean coherent scattering domain size distribution as defined in *NEWMOD2*, Tr = trace.

standpoint of uplift cycling of cationic nutrients (i.e. K⁺), the selectivity of microbial communities in contact with specific mineral surfaces, as shown by Lybrand et al. (2017), is important to both the early stages of mineral weathering and the late stages of establishing well defined argillic horizons.

The modeled abundances of mixed-layer clays in the Calhoun CZO supports the notion that they are present at both shallow and deep levels in the weathering profiles and often comprise >50% of the clay mineral assemblage (Table 3 and Fig. 6). From the standpoint of exchangeable sites for nutrients sources and sinks, 2:1 layer types (i.e. B+S+I+V+H) have a greater capacity than 1:1 layer types (i.e. K) because of redox-induced changes in layer charge stemming from octahedral iron. The mechanism for this process, as proposed by Stucki (1988), involves uptake of cationic species coupled to structural Fe reduction during seasonal wet periods and release of cationic species coupled to structural Fe oxidation during seasonal dry periods (See also Barcellos et al. 2018). Wetting and drying cycles in surface conditions have been shown to increase the abundance of illite in Fe-rich I-S mixed-layer clays, and that this process is only partially reversible (Huggett & Cuadros 2005; Ramirez et al. 2005). The current working hypothesis is that the cation exchange capacity of the samples with more abundant 2:1 layer types would be greater than those with fewer 2:1 layer types.

Deep samples at the CCZO have a relatively greater number of 2:1 layer types than equivalent shallow samples, for both forested and cultivated settings. The cultivated site situated lower in landscape position (R1C3) has a greater number of 2:1 layer types than the cultivated site higher in landscape position (R1C2). The weathering profiles in the forested site have a greater number of 2:1 layer types than the cultivated site. These trends point to factors that Jenny (1941) established long ago, whereby variations in climate, parent material, topography, biota, and time all have an influence on the suite of minerals that are present in a soil. The exact mechanisms by which mixed-layer clays form has been a challenge to understand, but the nature of interlayer cations has been deemed important (Le Dred 1978; Lanson 2011; Viennet et al. 2015). Through the multiple saturation approach and modeling results in this study, evidence is now provided that supports the idea that land cover and landscape position are causative factors in

Table 3 Summation of layer type abundances from all discrete and mixed-layer phases

Sample	Layer Type	Abundance (wt. %)			
		Mg-sat/ EG	Mg-sat/ 110 C	K-sat/ EG	K-sat/ 110 C
R1C2_13-80	Kaolinite	90	85	87	86
	Illite-like	7	9	9	10
	Vermiculite	1	3	3	3
	Smectite	0	0	0	0
	HIV	1	1	1	1
R1C2_700-800	Kaolinite	75	68	61	72
	Illite-like	17	32	36	28
	Vermiculite	8	0	3	0
	Smectite	0	0	0	0
	HIV	0	0	0	0
R1C3_58-86	Kaolinite	89	87	89	84
	Illite-like	7	9	8	11
	Vermiculite	2	3	3	4
	Smectite	0	0	0	0
	HIV	1	1	1	1
R1C3_600-650	Kaolinite	65	67	63	67
	Illite-like	29	28	34	30
	Vermiculite	5	4	3	2
	Smectite	1	1	0	0
	HIV	0	0	0	0
R7P2_57-82	Kaolinite	86	86	86	86
	Illite-like	10	10	11	11
	Vermiculite	3	3	3	3
	Smectite	0	0	0	0
	HIV	1	1	1	0
R7P2_700-800	Kaolinite	67	65	67	76
	Illite-like	25	27	28	24
	Vermiculite	1	8	5	0
	Smectite	7	0	0	0
	HIV	0	0	0	0

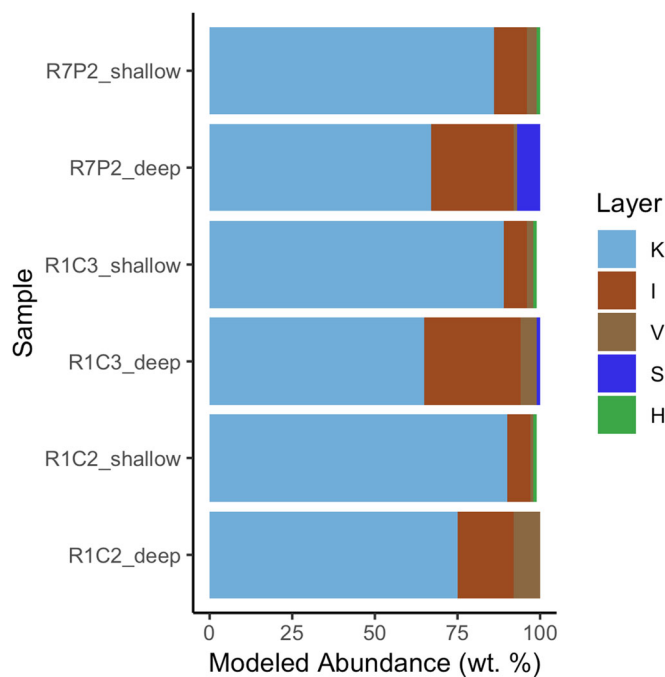


Fig. 6 Modeled abundance (wt.%) of layer types in each sample. K = kaolinite, I = illite-like, V = vermiculite, S = smectite, H = HIV. See text, which highlights general trends of greater abundance of 2:1 clays (I+V+S+H) at deep in all of the profiles and greater abundance of smectitic layers in the forested site and cultivated site situated lower in landscape position

642 formation of the mixed-layer mineral assemblages. Further-
 643 more, the presence of mixed-layer clays and landscape man-
 644 agement influence the cycling and fate of transport of potassiu-
 645 m in temperate climate ecosystems. Samples deep in the
 646 profile of the cultivated site higher on the landscape (R1C2)
 647 show the least abundance of 2:1 layer types. The deep samples
 648 from the cultivated site lower in landscape position (R1C3) has
 649 nearly the same overall abundance of 2:1 layer types as the profile
 650 higher in the landscape, but the 2:1 layer types are smectitic.
 651 The pine plot exhibited the most abundant expandable layers
 652 (modeled as smectite and vermiculite) deep in the profile,
 653 particularly when compared to the deep cultivated site.

654 Comparing the shallow samples across all sites reveals they
 655 all have HIV present, which is common in the A-horizons and
 656 upper B-horizons of soils in this region (Barnhisel and Bertsch
 657 1989; Schroeder et al. 1997). The forested site contains a greater
 658 amount of 2:1 clay layer types than the cultivated sites, thus
 659 favoring a larger pool in forested soils for sourcing/sinking cation
 660 nutrients. This is independently supported by total potassium
 661 concentrations measured in each profile (see Fig. S8). Averaging
 662 the bulk wt.% K₂O in the upper 0–100 cm reveals an increasing
 663 trend of 0.18 to 0.48 to 1.00 wt.% K₂O for R1C2, R1C3, and
 664 R7P2, respectively. Whereas for the deeper 100–700 cm the
 665 averaged K₂O contents trend from 1.18 to 0.55 to 0.63 wt.%
 666 for R1C2, R1C3, and R7P2, respectively. Some lithologic control
 667 on these trends is likely, however the larger K₂O contents of the
 668 pine site surface soils supports the notion that greater amounts of
 669 potassium are being retained, compared to the cultivated sites.
 670 Furthermore, the cultivated site highest in landscape position has
 671 the lowest concentrations of K₂O. These trends agree with the

672 expected increase in leaching and decrease in near-surface addi-
 673 tion of K⁺ hypothesized to occur via potassium uplift (Jobbagy
 674 and Jackson 2004; Balogh-Brunstad et al. 2008). A further
 675 hypothesis is that equivalent sites forested with older hardwoods
 676 would have similar abundances of 2:1 layer types in shallow
 677 portions of their profile and greater abundances deep in the
 678 profile compared with pine and cultivated sites, thus collectively
 679 creating important pools for cation source/sink cycling, under all
 680 other equivalent soil forming conditions (Schroeder 2018).

681 This more highly detailed analysis of mixed-layer types
 682 presented herein helps to define more accurately the mecha-
 683 nisms by which the K⁺ nutrient uplift process works, particu-
 684 larly as discussed by Austin et al. (2018), Bacon (2014), and
 685 Richter & Markewitz (1995). Proposed here is that the ex-
 686 change sites in the mixed-layer clays offer a refugium for K⁺
 687 (and possible NH₄⁺) as nutrients that are returned to the soil
 688 from decaying plant matter during the winter season. The
 689 wetter soil conditions during the winter promote reducing soil
 690 conditions, which increases negative layer charge in the
 691 mixed-layer clays. Cations compensate for this layer charge
 692 difference, which serve to store in the interlayer sites. Seasonal
 693 drying of the soils onsets oxidation of the mixed-layer clays,
 694 which decreases layer charge and results in the release of stored
 695 interlayer cations, with subsequent availability of cation nutri-
 696 ents for uptake by plants during their growing season.

697 CONCLUSIONS

698 Using *NEWMOD2* to simulate XRD patterns and quantify
 699 the relative abundances of mixed-layer clays in various

700 saturation and hydration states from the CCZO revealed that
 701 land use and landscape position are causative factors in deter-
 702 mining the differences in the mineral assemblages. The mixed-
 703 layer clay assemblages comprise a variety of 2:1 layer types
 704 (biotite, illite-like, vermiculite, smectite, and hydroxy-interlayer-
 705 vermiculite) and 1:1 layer types (kaolinite), all with variable
 706 ranges of layer types/proportions, ordering, and mean crystal
 707 size domains, depending on depth in profile, landscape position,
 708 and land use. A general trend of more 2:1 layer types with
 709 exchangeable sites in the mixed-layering occurs in the lower
 710 landscape position, relative to the higher landscape position. A
 711 general trend of more 2:1 layer types in the mixed-layering
 712 occurs in the forested locations than cultivated locations.

713 This leads to a generalization that management of upland
 714 cultivated sites in the S.E. US. Piedmont has less capacity than
 715 management of forested sites to serve as pools for storage of
 716 cations such a potassium. Potassium and other nutrients are
 717 hypothesized to be seasonally uplifted and cycled in soils.
 718 Primary minerals, biotite and feldspar, are hydrolized and/or
 719 transformed to create secondary mixed-layer clays. The second-
 720 ary mixed-layer clays further undergo continued redox,
 721 hydrolysis, and transformation to generate other forms of
 722 mixed-layer clay. Independent measures of bulk potassium
 723 content from the samples studied showed greater concentra-
 724 tions in the forested sites near the surface compared with the
 725 cultivated sites. Of the two cultivates sites, the site lower in
 726 landscape position has greater concentrations near the surface
 727 compared with the site higher in landscape position. XRD
 728 assessment of soil clay-mineral assemblages in the critical
 729 zone, using multiple cation saturation state and modeling, is
 730 essential for quantifying the pools for cation nutrients, such as
 731 potassium. These mixed-layer clays are key components to the
 732 proposed mechanism for K⁺ uplift concepts.

733

734 ACKNOWLEDGEMENTS

735 This work was supported by NSF grant EAR-GEO-1331846.
 736 Thanks are given the entire team of Calzoners, who can be recog-
 737 nized at <http://criticalzone.org/calhoun/people/>. The authors thank
 738 Will Cook for data archiving and management of the 2016 Big Dig
 739 program. Appreciation is also extended to anonymous reviewers
 740 and editors that provided valuable feedback.

741

742 Compliance with Ethical Standards

743 Conflicts of Interest

744 The authors declare that they have no conflicts of interest.

745

746

748

747

748 REFERENCES

749 Austin, J., Perry, A., Richter, D. D., & Schroeder, P. (2018).
 750 Modifications of 2:1 clay minerals in a kaolinite-dominated Ultisol
 751 under changing land-use regimes. *Clays and Clay Minerals*, 66, 61–
 752 73.
 753 Bacon, A. R., Richter, D. D., Bierman, P. R., & Hood, D. H. (2012).
 754 Coupling meteoric ¹⁰Be with pedogenic losses of ⁹Be to improve

soil residence time estimates on an ancient North American soil. *755*
Geology, 40, 847–850. *756*
 Balogh-Brunstad, Z., Keller, C. K., Bormann, B. T., O'Brien, R., Wang, *757*
 D., & Hawley, G. (2008). Chemical weathering and chemical de- *758*
 nudation dynamics through ecosystem development and distur- *759*
 bance. *Global Biogeochemical Cycles*, 22, 11. *760*
 Barcellos, D., Cyle, K. T., & Thompson, A. (2018). Faster redox *761*
 fluctuations can lead to higher iron reduction rates in humid forest *762*
 soils. *Biogeochemistry*, 137, 367–378. *763*
 Barnhisel, R. I., & Bertsch, P. M. (1989). Chlorites and hydroxy- *764*
 interlayered vermiculite and smectite. In J. B. Dixon & S. B. *765*
 Weed (Eds.), *Minerals in Soil Environments* (pp. 729–788). *766*
 Maddison, Wisconsin: Soil Science Society of America. *767*
 Barre, P., Montagnier, C., Chenu, C., Abbadie, L., & Velde, B. (2008). *768*
 Clay minerals as a soil potassium reservoir: Observation and quan- *769*
 tification through X-ray diffraction. *Plant and Soil*, 302, 213–220. *770*
 Barre, P., Velde, B., & Abbadie, L. (2007a). Dynamic role of "illite- *771*
 like" clay minerals in temperate soils: Facts and hypotheses. *772*
Biogeochemistry, 82, 77–88. *773*
 Barre, P., Velde, B., Catel, N., & Abbadie, L. (2007b). Soil-plant *774*
 potassium transfer: Impact of plant activity on clay minerals as seen *775*
 from X-ray diffraction. *Plant and Soil*, 292, 137–146. *776*
 Billings, S.A., Hirmas, D., Sullivan, P.L., Lehmeier, C.A., Bagchi, S., *777*
 Min, K., Brecheisen, Z., Hauser, E., Stair, R., Flourmoy, R., & *778*
 Richter, D.D. (2018). Loss of deep roots limits biogenic agents of *779*
 soil development that are only partially restored by decades of forest *780*
 regeneration. *Elementa-Science of the Anthropocene*, 6. *781*
 Comu, S., Montagne, D., Hubert, F., Barre, P., & Caner, L. (2012). *782*
 Evidence of short-term clay evolution in soils under human impact. *783*
Comptes Rendus Geoscience, 344, 747–757. *784*
 Diaz, M., Robert, J. L., Schroeder, P. A., & Prost, R. (2010). Far- *785*
 infrared study of the influence of the octahedral sheet composition *786*
 on the K⁺-layer interactions in synthetic phlogopites. *Clays and* *787*
Clay Minerals, 58, 263–271. *788*
 Dumon, M., & Van Ranst, E. (2016). Pyxrd v0.6.7: A free and open- *789*
 source program to quantify disordered phyllosilicates using multi- *790*
 specimen X-ray diffraction profile fitting. *Geoscientific Model* *791*
Development, 9, 41–57. *792*
 Gier, S., Ottner, F., & Johns, W. D. (1998). Layer-charge heterogeneity *793*
 in smectites of I-S phases in pelitic sediments from the molasse *794*
 basin, Austria. *Clays and Clay Minerals*, 46, 670–678. *795*
 Hillier, S., & Butler, B. (2018). New XRD data-based approaches to *796*
 soil mineralogy. *Spectroscopy*, 33, 34–36. *797*
 Hochella, M. F., Mogk, D. W., Ranville, J., Allen, I. C., Luther, G. W., *798*
 Marr, L. C., McGrail, B. P., Murayama, M., Qafoku, N. P., Rosso, K. *799*
 M., Sahai, N., Schroeder, P. A., Vikesland, P., Westerhoff, P., & *800*
 Yang, Y. (2019). Natural, incidental, and engineered nanomaterials *801*
 and their impacts on the Earth system. *Science*, 363, 1414. *802*
 Huggett, J. M., & Cuadros, J. (2005). Low-temperature illitization of *803*
 smectite in the late eocene and early oligocene of the Isle of Wight *804*
 (Hampshire Basin), UK. *American Mineralogist*, 90, 1192–1202. *805*
 Jenny, H. (1941). *Factors of Soil Formation: A system of Quantitative* *806*
Pedology (p. 281). New York: Dover Publications. *807*
 Jobbagy, E. G., & Jackson, R. B. (2004). The uplift of soil nutrients by *808*
 plants: Biogeochemical consequences across scales. *Ecology*, 85, *809*
 2380–2389. *810*
 Joussein, E., Petit, S., Churchman, J., Theng, B., Righi, D., & Delvaux, *811*
 B. (2005). Halloysite clay minerals – A review. *Clay Minerals*, 40, *812*
 383–426. *813*
 Lagaly, G. (1982). Layer charge heterogeneity in vermiculites. *Clays* *814*
and Clay Minerals, 30, 215–222. *815*
 Lanson, B. (2011). Modelling of X-ray diffraction profiles: *816*
 Investigation of defect lamellar structure crystal chemistry. Pp. *817*
 151–190 in: *Layered Mineral Structures and their Application in* *818*
Advanced Technologies (M.F. Brigatti, and A. Mottana, editors), 11, *819*
 European Mineralogical Union and the Mineralogical Society of *820*
 Great Britain & Ireland, London. *821*
 Lanson, B., Sakharov, B. A., Claret, F., & Drits, V. A. (2009). *822*
 Diagenetic smectite-to-illite transition in clay-rich sediments: A *823*

- 824 reappraisal of X-ray diffraction results using the multi-specimen
825 method. *American Journal of Science*, 309, 476–516.
- 826 Le Dred, R. (1978). Formation De Complexes Mica-vermiculite-
827 halogenure De Metal Alcalin. *Clay Minerals*, 13, 187–197.
- 828 Lybrand, R., Austin, J., Schroeder, P.A., Zaharescu, D., & Gallery, R.
829 (2017). Cross-scale perspectives on mineral weathering in the critical
830 zone. Paper no. 195-13 in: *Abstracts with Programs - Geological Society of America*. 49, Seattle, Washington, USA.
- 831 Lybrand, R.A., Austin, J.C., Fedenko, J., Gallery, R.E., Rooney, E.,
832 Schroeder, P.A., Zaharescu, D.G., & Qafoku, O. (2019). A coupled
833 microscopy approach to assess the nano-landscape of weathering.
834 *Scientific Reports*, 9.
- 835 MacEwan, D. M. C., & Wilson, M. J. (1980). *Crystal Structures of*
836 *Clay Minerals and their X-ray Identification*. London:
837 Mineralogical Society.
- 838 Meunier, A. (2007). Soil hydroxy-interlayered minerals: A re-
839 interpretation of their crystallochemical properties. *Clays and Clay*
840 *Minerals*, 55, 380–388.
- 841 Officer, S. J., Tillman, R. W., Palmer, A. S., & Whitton, J. S. (2006).
842 Variability of clay mineralogy in two new zealand steep-land top-
843 soils under pasture. *Geoderma*, 132, 427–440.
- 844 Ramirez, S., Righi, D., & Petit, S. (2005). Alteration of smectites
845 induced by hydrolytic exchange. *Clay Minerals*, 40, 15–24.
- 846 Reynolds Jr., R. C. (1980). Interstratified clay minerals. In G. W.
847 Brindley & G. Brown (Eds.), *Crystal Structures of Clay Minerals*
848 *and their X-ray Identification* (pp. 249–303). London:
849 Mineralogical Society.
- 850 Reynolds, R. C. (1985). *Newmod a computer program for the calcu-*
851 *lation of one-dimensional X-ray diffraction patterns of mixed-*
852 *layered clays*. Hanover, NH: Pp., R.C. Reynolds Jr.
- 853 Reynolds, R. C. (1986). The lorentz-polarization factor and preferred
854 orientation in oriented clay aggregates. *Clays and Clay Minerals*,
855 34, 359–367.
- 856
- 857 Richter, D., & Markewitz, D. (1995). How deep is soil? *BioScience*,
858 45, 600–699.
- 859 Schroeder, P. A. (1992). Far-infrared study of the interlayer torsional-
860 vibrational mode of mixed-layer illite smectites. *Clays and Clay*
861 *Minerals*, 40, 81–91.
- 862 Schroeder, P. A. (2018). *Clays in the Critical Zone*. Cambridge:
863 Cambridge University Press.
- 864 Schroeder, P. A., Kim, J. G., & Melear, N. D. (1997). Mineralogical
865 and textural criteria for recognizing remnant cenozoic deposits on
866 the piedmont: Evidence from Sparta and Greene County, Georgia,
867 USA. *Sedimentary Geology*, 108, 195–206.
- 868 Smith, D. W. (1977). Ionic hydration enthalpies. *Journal of Chemical*
869 *Education*, 54, 540.
- 870 Stucki, J. W. (1988). Structural iron in smectites. In J. W. Stucki, B. A.
871 Goodman, & U. Schwertmann (Eds.), *Iron in Soils and Clay*
872 *Minerals* (Vol. 217, pp. 625–676). Dordrecht, The Netherlands:
873 Springer.
- 874 Toby, B. H. (2006). R factors in Rietveld analysis: How good is good
875 enough? *Powder Diffraction*, 21, 67–70.
- 876 Trimble, S.W. (2008). *Man-induced soil erosion on the southern pied-*
877 *mont, 1700–1970*. Pp. 70. Soil and Water Conservation Society,
878 Department of Geography, UCLA, Los Angeles, California, USA.
- 879 Yuan, H., & Bish, D. L. (2010). NEWMOD plus, a new version of the
880 NEWMOD program for interpreting X-ray powder diffraction pat-
881 terns from interstratified clay minerals. *Clays and Clay Minerals*,
882 58, 318–326.
- 883 Viennet, J.-C., Hubert, F., Ferrage, E., Tertre, E., Legout, A., &
884 Turpault, M.-P. (2015). Investigation of clay mineralogy in a tem-
885 perate acidic soil of a forest using X-ray diffraction profile model-
886 ing; beyond the HIS and HIV description. *Geoderma*, 241, 75–86.
- (Received 21 May 2019; revised 6 December 2019; accepted 18
887 December 2019)
- 888

AUTHOR QUERY

AUTHOR PLEASE ANSWER QUERY.

- Q1. Ref. "Bacon (2014)" is cited in the body but its bibliographic information is missing. Kindly provide its bibliographic information in the list.

UNCORRECTED PROOF